J Eng Math (2011) 71:15–30
DOI 10.1007/s10665-010-9421-9

Electro-osmotic flow of viscoelastic fluids in microchannels under asymmetric zeta potentials

A. M. Afonso · M. A. Alves · F. T. Pinho

Received: 27 January 2010 / Accepted: 22 September 2010 / Published online: 11 November 2010

Abstract The flow of viscoelastic fluids between parallel plates under the combined influence of electro-osmotic and pressure gradient forcings with asymmetric boundary conditions, by considering different zeta potentials at the walls, is investigated. The fluids are z–z symmetric electrolytes. The analytic solutions of the electrical potential, velocity distributions and streaming potential are based on the Debye–Hückel approximation for weak potential. The viscoelastic fluids used are modelled by the simplified Phan-Thien–Tanner constitutive equation, with linear kernel for the stress coefficient function, and the Finitely Extensible Nonlinear Elastic dumbbells model with a Peterlin approximation for the average spring force. The combined effects of fluid rheology, electrical double-layer thickness, ratio of the wall zeta potentials and ratio between the applied streamwise gradients of electrostatic potential and pressure on the fluid velocity and stress distributions are discussed.

Keywords Electro-osmotic/pressure driven flows · Finitely Extensible Nonlinear Elastic model-Peterlin's approximation (FENE-P) · Simplified Phan-Thien–Tanner model (sPTT) · Viscoelastic fluids

1 Introduction

Soong and Wang [1] investigated electro-kinetic effects on flow and heat transfer of Newtonian liquids flowing between two parallel plates subject to asymmetric boundary conditions including wall-sliding motion, different zeta potentials, and unequal heat fluxes at the walls. They showed that the surface electric condition due to unequal zeta potentials dramatically influences the electric potential distribution with concomitant changes in the streaming potential and the Newtonian fluid-flow characteristics. Such asymmetries are actually fairly normal because many

A. M. Afonso · M. A. Alves
Departamento de Engenharia Química, Centro de Estudos de Fenómenos de Transporte, Faculdade de Engenharia da Universidade do Porto, Rua Dr. Roberto Frias s/n, 4200-465 Porto, Portugal
e-mail: aafonso@fe.up.pt

M. A. Alves
e-mail: mmalves@fe.up.pt

F. T. Pinho (✉)
Departamento de Engenharia Mecânica, Centro de Estudos de Fenómenos de Transporte, Faculdade de Engenharia da Universidade do Porto, Rua Dr. Roberto Frias s/n, 4200-465 Porto, Portugal
e-mail: fpinho@fe.up.pt

manufacturing techniques use different materials at different walls [2]. For instance, in soft lithography the channels are often made of polydimethylsiloxane (PDMS) except for the top wall that is often made of glass for optical access or other material for other purpose. In pure electro-osmosis the consequence of this is a linear velocity profile in the bulk instead of a constant front [3]. Asymmetric electro-osmosis can also be the outcome of imposed polarization by AC fields in otherwise symmetric geometries [4,5], but this matter is outside the scope of this work which assumes DC currents.

In DC electro-osmosis, recently an investigation was carried out by Afonso et al. [6], who presented the analytical solutions for channel and pipe flows of viscoelastic fluids under the mixed influence of electro-osmotic and pressure-gradient forcing but only under symmetric boundary conditions. To describe viscoelasticity they used the simplified Phan-Thien and Tanner model (sPTT model, [7]), with linear kernel for the stress-coefficient function and zero second normal-stress difference [8], and the Finitely Extensible Nonlinear Elastic dumbbells model with a Peterlin approximation for the average spring force (FENE-P model) [9]. Subsequently, a similar investigation was carried out by Dhinakaran et al. [10] for PTT fluids with non-zero second normal-stress-difference coefficient in shear flowing between parallel plates, which identified the conditions for the onset of an instability originated in the constitutive equation. Both analyses were restricted to cases with small electric double layers, where the distance between the walls of a microfluidic device is at least one order of magnitude larger than the thickness of the electric double layer (EDL). When the viscoelastic flow is induced by a combination of both electrical and pressure potentials, as in the investigations by Afonso et al. [6], in addition to the independent contributions from these two mechanisms, there is an extra term in the velocity profile that simultaneously combines both, which is absent for the Newtonian case where the superposition principle applies. This nonlinear term can contribute significantly to the total flow rate, depending on the value of the EDL thickness and is a consequence of the nonlinear nature of the constitutive relation of the fluid. Park and Lee [11] derived expressions for the Helmholtz–Smoluchowski velocity for pure electro-osmotic flow of PTT fluids and provided a simple numerical procedure to calculate its value, and Sousa et al. [12] considered the effect of a Newtonian skimming layer for the PTT fluid. Note that earlier investigations on purely electro-osmotic flow or combined electro-osmosis with pressure-gradient forcing were carried out in the context of Newtonian fluids, as reviewed by Afonso et al. [6]. However, the contributions reviewed in that paper are all for symmetric zeta potentials.

This work aims to generalize the study of symmetric z–z electrolyte viscoelastic fluids in electro-osmotic/pressure-gradient-driven flows to other practical relevant flow conditions by presenting the analytical solutions for the flows of sPTT and FENE-P fluids between two parallel plates under asymmetric boundary conditions of unequal zeta potentials at the channel walls. Dilute and semi-dilute polymer solutions can easily be represented by these constitutive equations. Specifically, in [13] the rheology of various aqueous solutions of polyethylene oxide, with molecular weights ranging from 2×10^6 to 8×10^6 g/mol, and of an 18×10^6 g/mol polyacrylamide, all at concentrations not exceeding 0.1% by weight, were investigated. The rheologies of these fluids were very well fitted by a single-mode form of the PTT model, which is quite adequate for this shear flow.

The paper starts with the set of governing equations including the nonlinear Poisson–Boltzmann equation governing the EDL fields and the momentum equation modified by the body force associated with the applied electrical potential field. The simplifications required to obtain the analytical solution are discussed, the solutions are presented and a discussion of the effects of the various relevant nondimensional parameters upon the flow characteristics closes this work. The particular case of streaming potential is presented in Appendix A.

2 Governing equations

The basic equations describing the flow are the continuity equation,

$$\nabla \cdot \mathbf{u} = 0 \tag{1}$$

and the momentum equation,

$$\rho \frac{\mathrm{D}\mathbf{u}}{\mathrm{D}t} = \nabla \cdot \boldsymbol{\tau} - \nabla p + \mathbf{F}, \tag{2}$$

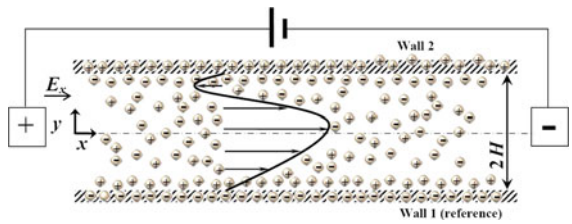

Fig. 1 Schematic of the flow in a parallel plate microchannel

where $\mathbf{u}$ is the velocity vector, p the pressure, t the time, ρ the fluid density (assumed constant) and $\boldsymbol{\tau}$ the polymeric extra stress contribution. The body force $\mathbf{F}$ in the momentum equation (2) is here given as

$$\mathbf{F} = \rho_e \mathbf{E}, \tag{3}$$

where $\mathbf{E}$ is the applied external electric field and ρ_e is the net electric-charge density associated with the spontaneously formed electric double layers, which are assumed here not to be affected by the imposed electric field. The electric field is related to a potential (Φ), by $\mathbf{E} = -\nabla\Phi$, with $\Phi = \psi + \phi$, where ϕ is the applied streamwise potential and ψ is the equilibrium induced potential at the channel walls, associated with the interaction between the ions of the fluid and the dielectric properties of the wall. The boundary conditions are no-slip at both walls and asymmetric zeta potentials at the walls, with Fig. 1 showing schematically the flow channel, coordinate system and type of forcing.

2.1 Constitutive equations

2.1.1 sPTT model

One of the viscoelastic models adopted here to represent viscoelastic effects is the sPTT equation (simplified Phan-Thien and Tanner [7]), which can be expressed by

$$f(\tau_{kk})\boldsymbol{\tau} + \lambda \overset{\nabla}{\boldsymbol{\tau}} = 2\eta \mathbf{D}, \tag{4}$$

where $\mathbf{D}$ is the rate-of-deformation tensor, $\mathbf{D} = \frac{1}{2}\left(\nabla\mathbf{u} + \nabla\mathbf{u}^{\mathrm{T}}\right)$, λ is a relaxation time, η is the constant viscosity coefficient of the model and $\overset{\nabla}{\boldsymbol{\tau}}$ represents the upper-convected derivative, defined by

$$\overset{\nabla}{\boldsymbol{\tau}} = \frac{\mathrm{D}\boldsymbol{\tau}}{\mathrm{D}t} - \nabla\mathbf{u}^{\mathrm{T}} \cdot \boldsymbol{\tau} - \boldsymbol{\tau} \cdot \nabla\mathbf{u}. \tag{5}$$

The stress-coefficient function, $f(\tau_{kk})$, can be expressed in linearised form as

$$f(\tau_{kk}) = 1 + \frac{\varepsilon\lambda}{\eta}\tau_{kk}, \tag{6}$$

where $\tau_{kk} = \tau_{xx} + \tau_{yy} + \tau_{zz}$ is the trace of the extra stress tensor.

2.1.2 FENE-P model

Another viscoelastic model used in this work is the FENE-P constitutive equation, based on the kinetic theory for finitely extensible dumbbells with a Peterlin closure for the average spring force [9]. The coarse-grained molecule of the FENE-P model is represented by a single dumbbell, whose connector force follows a nonlinear spring law possessing limited extension, without consideration for excluded-volume effects and hydrodynamic interaction. The resulting constitutive equation for the polymer stress can be written as

$$Z(\tau_{kk})\boldsymbol{\tau} + \lambda \overset{\nabla}{\boldsymbol{\tau}} - \lambda\left(\boldsymbol{\tau} - \frac{b}{b+2} nk_B T \mathbf{I}\right)\frac{\mathrm{D}\log Z}{\mathrm{D}t} = 2\frac{b}{b+2} nk_B T \lambda \mathbf{D}, \tag{7}$$

where $\overset{\nabla}{\boldsymbol{\tau}}$ represents the upper-convected derivative defined by (4), b is a parameter that measures the extensibility of the dumbbell, k_B is the Boltzmann constant, T is the absolute temperature and n is a parameter of the model [9]. The stress-coefficient function, $Z(\tau_{kk})$ can be expressed as

$$Z(\tau_{kk}) = 1 + 3\left(\frac{1}{b+2} + \frac{\lambda}{3\eta}\frac{\tau_{kk}}{(b+5)}\right). \tag{8}$$

2.2 Poisson–Boltzmann equation

If a liquid contacts a dielectric surface there are interactions between the ions and the wall, leading to a spontaneous charge distribution at the fluid and the wall. The wall acquires a charge and the counter-ions in the fluid are attracted by the wall while the co-ions are repelled. In this case, an electric layer is formed near the wall, which is called the electric double layer (EDL, see [14] for more details). The induced potential field within the electric double layer, can be expressed by means of a Poisson equation:

$$\nabla^2\psi = -\frac{\rho_e}{\epsilon}, \tag{9}$$

where ψ denotes the EDL potential and ϵ is the dielectric constant of the solution. The net electric-charge density in the fluid, ρ_e, can be described by the following Boltzmann distribution

$$\rho_e = -2n_o ez \sinh\left(\frac{ez}{k_B T}\psi\right), \tag{10}$$

where n_o is the ion density, e is the electronic charge and z the valence of the ions. In order to obtain the velocity field, first we need to solve for the net charge-density distribution (ρ_e). The charge-density field can be calculated by combining (9), which for fully developed steady flow reduces to

$$\frac{\mathrm{d}^2\psi}{\mathrm{d}y^2} = -\frac{\rho_e}{\epsilon}, \tag{11}$$

and Eq. 10 to obtain the well-known Poisson–Boltzmann equation,

$$\frac{\mathrm{d}^2\psi}{\mathrm{d}y^2} = \frac{2n_o ez}{\epsilon}\sinh\left(\frac{ez}{k_B T}\psi\right). \tag{12}$$

The electro-osmotic flow is primarily caused by the movement of the charged species adjacent to the channel walls when subjected to an externally applied electric field. In general, the distribution of the charged species in the domain is governed by the potential at the walls and by the externally applied electric field. However, when the EDL thickness is small and the charge at the walls is not large, this distribution is essentially governed by the potential at the wall, ψ_0, and is not affected by the externally applied electric field. Thus, the charge distribution near the walls can be determined independently of the applied external electric field. In fact, the effect of fluid motion on the charge redistribution can itself be neglected when the fluid velocity is small, i.e., when the inertial terms in the momentum equation are not dominant or when the EDL thickness is small since the flow is locally uni-directional. In this work with the additional consideration of steady fully developed channel flow and the inherent symmetry, the charge redistribution is exactly null as is also the inertial term of the momentum equation. Then, for small values of ψ, it is also possible to conduct further simplifications because the Debye–Hückel linearization principle ($\sinh x \approx x$) can be invoked. Physically, this means that the electrical potential is small compared with the thermal energy of the ions, and the Poisson Boltzmann equation for the channel flow under investigation becomes:

$$\frac{\mathrm{d}^2\psi}{\mathrm{d}y^2} = \kappa^2\psi, \tag{13}$$

where $\kappa^2 = \frac{2n_o e^2 z^2}{\epsilon k_B T}$ is the Debye–Hückel parameter, associated with the thickness of the Debye layer, $\xi = \frac{1}{\kappa}$ (normally referred to as the EDL thickness). This approximation is valid when the Debye thickness is small but finite, i.e., for $10 \lesssim H/\xi \lesssim 10^3$.

Equation (13) can be integrated coupled with boundary conditions for different zeta potential at the walls, $\psi_{\|y=-H} = \zeta_1$ and $\psi_{\|y=H} = \zeta_2$ (cf. Fig. 1), leading to:

$$\psi(y) = \zeta_1 \left(\Psi_1 \mathrm{e}^{\kappa y} - \Psi_2 \mathrm{e}^{-\kappa y}\right) \tag{14}$$

with $\Psi_1 = \frac{(R_\zeta \mathrm{e}^{\kappa H} - \mathrm{e}^{-\kappa H})}{2\sinh(2\kappa H)}$ and $\Psi_2 = \frac{(R_\zeta \mathrm{e}^{-\kappa H} - \mathrm{e}^{\kappa H})}{2\sinh(2\kappa H)}$, and where $R_\zeta = \zeta_2/\zeta_1$ denotes the ratio of zeta potentials of the two walls. This equation is valid for $-H \leq y \leq H$ and, when $R_\zeta = 1$, the symmetric potential profile of Afonso et al. [6] is recovered.

Finally, the net charge-density distribution, Eq. 10, in conjunction with (14) reduces to

$$\rho_e = -\epsilon\kappa^2\zeta_1 \left(\Psi_1 \mathrm{e}^{\kappa y} - \Psi_2 \mathrm{e}^{-\kappa y}\right) = -\epsilon\kappa^2\zeta_1 \Omega_1^-(y), \tag{15}$$

where the operator $\Omega_p^{\pm}(y) = \Psi_1^p \left(\mathrm{e}^{\kappa y}\right)^p \pm \Psi_2^p \left(\mathrm{e}^{-\kappa y}\right)^p$ is a hyperbolic function of the transverse variable y which depends on the ratio of zeta potentials and on the thickness of the Debye layer.

3 Analytical solution

3.1 sPTT constitutive equation

The predictions of the sPTT model in this flow, for which $\mathbf{u} = \{u(y), 0, 0\}$, can be obtained from (5) and (6), yielding:

$$f(\tau_{kk})\tau_{xx} = 2\lambda\dot{\gamma}\tau_{xy}, \tag{16}$$

$$f(\tau_{kk})\tau_{xy} = \eta\dot{\gamma}, \tag{17}$$

where $\tau_{kk} = \tau_{xx}$ is the trace of the stress tensor and $\dot{\gamma} = \mathrm{d}u/\mathrm{d}y$ is the velocity gradient. The demonstration that $\tau_{yy} = 0$ for sPTT fluids in fully developed shear flows can be found in [15], so the stress-coefficient function becomes an explicit function of the normal stress τ_{xx} only. Upon division of the expressions for the two nonvanishing stresses (Eqs. 16, 17) the specific function $f(\tau_{xx})$ cancels out, and a relation between the non-zero normal and shear stresses is obtained:

$$\tau_{xx} = 2\frac{\lambda}{\eta}\tau_{xy}^2. \tag{18}$$

3.2 FENE-P constitutive equation

For the FENE-P fluid in fully developed channel flow, i.e., subjected to $\mathbf{u} = \{u(y), 0, 0\}$, Eqs. 7 and 8 reduce to

$$Z(\tau_{kk})\tau_{xx} = 2\lambda\dot{\gamma}\tau_{xy}, \tag{19}$$

$$Z(\tau_{kk})\tau_{xy} = \left(\frac{b+5}{b+2}\right)\eta\dot{\gamma}. \tag{20}$$

Again, the trace of the extra-stress tensor becomes $\tau_{kk} = \tau_{xx}$, thus

$$Z(\tau_{xx}) = \left(\frac{b+5}{b+2}\right)\left[1 + \frac{\lambda}{\eta}\frac{(b+2)}{(b+5)^2}\tau_{xx}\right]. \tag{21}$$

The relation between the normal and shear stresses is,

$$\tau_{xx} = 2\frac{\lambda}{\eta}\left(\frac{b+2}{b+5}\right)\tau_{xy}^2. \tag{22}$$

Inspection of these expressions and those of Sect. 3.1 shows similarities between the sPTT and FENE-P stress distributions and this will have consequences as discussed in Sect. 3.4.

3.3 Analytical solution for the sPTT model

From the previous simplifications, the momentum equation (2), for fully developed channel flow reduces to

$$\frac{\mathrm{d}\tau_{xy}}{\mathrm{d}y} = -\rho_e E_x + p_{,x}, \tag{23}$$

where $p_{,x} \equiv \mathrm{d}p/\mathrm{d}x$, $E_x \equiv -\mathrm{d}\phi/\mathrm{d}x$ and ϕ is the electric potential of the applied external field, which is characterized by a constant streamwise gradient. Note that in this flow the external electrical field is positive according to Fig. 1, and negative otherwise. Using Eq. 15, Eq. 23 can now be integrated to yield the following distribution of shear stress resulting from a linear combination of the pressure-gradient and electric-field contributions,

$$\tau_{xy} = \epsilon\kappa\zeta_1 E_x \Omega_1^+(y) + p_{,x} y + \tau_1, \tag{24}$$

where τ_1 is a shear-stress integration constant to be quantified later from the boundary conditions.

By using the relationship between the normal and shear stresses, Eq. 18, an explicit expression for the normal stress component is also obtained:

$$\tau_{xx} = 2\frac{\lambda}{\eta}\left(\epsilon\kappa\zeta_1 E_x \Omega_1^+(y) + p_{,x} y + \tau_1\right)^2. \tag{25}$$

The square term in (25) introduces a contribution to the normal stress from the combined electro-osmotic and pressure forces. After combining (17), (24) and (25) we arrive to the velocity gradient distribution, given by

$$\dot{\gamma} \equiv \frac{\mathrm{d}u}{\mathrm{d}y} = \left[1 + 2\varepsilon\lambda^2\left(\tfrac{\epsilon E_x\zeta_1}{\eta}\kappa\Omega_1^+(y) + \tfrac{p_{,x}}{\eta}y + \dot{\gamma}_1\right)^2\right]\left(\tfrac{\epsilon E_x\zeta_1}{\eta}\kappa\Omega_1^+(y) + \tfrac{p_{,x}}{\eta}y + \dot{\gamma}_1\right), \tag{26}$$

where for compactness we have used the *shear-rate asymmetry coefficient* defined as $\dot{\gamma}_1 = \tau_1/\eta$. We note that this coefficient has no particular physical interpretation.

Equation (26) is integrated subject to the no-slip boundary condition at both walls ($u_{\|y=H} = u_{\|y=-H} = 0$) and the resulting velocity profile is

$$\begin{aligned}
u = {} & \dot{\gamma}_1 (y+H)\left(1 + 2\varepsilon\lambda^2\dot{\gamma}_1^2\right) + \left[\frac{\epsilon E_x\zeta_1}{\eta}\right]\left(1 + 6\dot{\gamma}_1^2\varepsilon\lambda^2\right)\Omega_{1,1}^-(y) \\
& + 2\varepsilon\lambda^2\left[\frac{\epsilon E_x\zeta_1}{\eta}\right]^2\kappa\dot{\gamma}_1\left(6\Psi_1\Psi_2\kappa\,(y+H) + \frac{3}{2}\Omega_{2,1}^-(y)\right) + 2\varepsilon\lambda^2\left[\frac{\epsilon E_x\zeta_1}{\eta}\right]^3\kappa^2\left(\frac{1}{3}\Omega_{3,1}^-(y) + 3\Psi_1\Psi_2\Omega_{1,1}^-(y)\right) \\
& + \frac{1}{2}\left[\frac{p_{,x}}{\eta}\right]\left(y^2 - H^2\right)\left(1 + 6\varepsilon\lambda^2\dot{\gamma}_1^2 + \varepsilon\lambda^2\left[\frac{p_{,x}}{\eta}\right]^2\left(y^2 + H^2\right)\right) \\
& + 2\dot{\gamma}_1\varepsilon\lambda^2\left[\frac{p_{,x}}{\eta}\right]^2\left(y^3 + H^3\right) + 12\frac{\varepsilon\lambda^2\left[\frac{\epsilon E_x\zeta_1}{\eta}\right]\left[\frac{p_{,x}}{\eta}\right]}{\kappa}\dot{\gamma}_1\left(\Omega_{1,2}^-(y) - \Omega_{1,1}^+(y)\right) \\
& + 6\frac{\varepsilon\lambda^2\left[\frac{\epsilon E_x\zeta_1}{\eta}\right]\left[\frac{p_{,x}}{\eta}\right]^2}{\kappa^2}\left(\Omega_{1,3}^-(y) + 2\Omega_{1,1}^-(y) - 2\Omega_{1,2}^+(y)\right) \\
& + 6\varepsilon\lambda^2\left[\frac{\epsilon E_x\zeta_1}{\eta}\right]^2\left[\frac{p_{,x}}{\eta}\right]\left(\Psi_1\Psi_2\kappa^2\left(y^2 - H^2\right) + \frac{1}{2}\Omega_{2,2}^-(y) - \frac{1}{4}\Omega_{2,1}^+(y)\right),
\end{aligned} \tag{27}$$

where the operator $\Omega_{p,q}^{\pm}(y)$ is defined as

$$\Omega_{p,q}^{\pm}(y) = (\kappa y)^{(q-1)}\,\Omega_p^{\pm}(y) - (-1)^{(q+1)}\,(\kappa H)^{(q-1)}\,\Omega_p^{\pm}(-H). \tag{28}$$

The no-slip boundary conditions for the velocity at the walls allows the determination of the integration constants. Here we choose to obtain an explicit form for $\dot{\gamma}_1$. The application of the second no-slip boundary condition leads to the following cubic equation:

$$\dot{\gamma}_1^3 + a_1\dot{\gamma}_1^2 + a_2\dot{\gamma}_1 + a_3 = 0. \tag{29}$$

The Cardan–Tartaglia solution of the cubic equation gives the following explicit expression for the physically meaningful real solution of (29) (the other two solutions are complex and unphysical),

$$\begin{aligned}
\dot{\gamma}_1 &= \sqrt[3]{-\frac{b_1}{2}+\sqrt{\frac{b_1^2}{4}+\frac{a^3}{27}}}+\sqrt[3]{-\frac{b_1}{2}-\sqrt{\frac{b_1^2}{4}+\frac{a^3}{27}}}-\frac{a_1}{3},\\
a &= a_2-\frac{a_1^2}{3},\\
b_1 &= a_3-\frac{a_1a_2}{3}+\frac{2a_1^3}{27},
\end{aligned} \tag{30}$$

with coefficients

$$\begin{aligned}
a_1 &= \frac{3}{2}\frac{\epsilon E_x\zeta_1}{\eta H}\Omega^-_{1,1}(H),\\
a_2 &= \frac{1}{2\varepsilon\lambda^2}+\left(\frac{p_{,x}}{\eta}\right)^2H^2+6\left(\frac{\epsilon E_x\zeta_1}{\eta}\kappa\right)^2\Psi_1\Psi_2+\frac{3}{4}\frac{\left(\frac{\epsilon E_x\zeta_1}{\eta}\kappa\right)^2}{\kappa H}\Omega^-_{2,1}(H)\\
&\quad+3\frac{\left(\frac{\epsilon E_x\zeta_1}{\eta}\kappa\right)\frac{p_{,x}}{\eta}}{\kappa^2H}\left(\Omega^-_{1,2}(H)-\Omega^+_{1,1}(H)\right),\\
a_3 &= \frac{1}{2}\frac{\epsilon E_x\zeta_1}{\eta}\frac{\Omega^-_{1,1}(H)}{2\varepsilon\lambda^2H}+\frac{1}{2}\frac{\left(\frac{\epsilon E_x\zeta_1}{\eta}\kappa\right)^3}{\kappa H}\left(\frac{1}{3}\Omega^-_{3,1}(H)+3\Psi_1\Psi_2\Omega^-_{1,1}(H)\right)\\
&\quad+\frac{3}{2}\frac{\left(\frac{\epsilon E_x\zeta_1}{\eta}\kappa\right)^2\frac{p_{,x}}{\eta}}{\kappa^2H}\left(\frac{1}{2}\Omega^-_{2,2}(H)-\frac{1}{4}\Omega^+_{2,1}(H)\right)+\frac{3}{2}\frac{\left(\frac{\epsilon E_x\zeta_1}{\eta}\kappa\right)\left(\frac{p_{,x}}{\eta}\right)^2}{\kappa^3H}\left(\Omega^-_{1,3}(H)+2\Omega^-_{1,1}(H)-2\Omega^+_{1,2}(H)\right).
\end{aligned} \tag{31}$$

As suggested by (27) there are terms which are only proportional to E_x, others to $p_{,x}$ and those that are simultaneously proportional to $p_{,x}$ and E_x. Even the terms proportional to $\dot{\gamma}_1$ depend on both forcings. Therefore, as discussed by Afonso et al. [6], the superposition principle valid for Newtonian fluids and quasi-linear viscoelastic fluids is no longer valid for the sPTT fluid and suggests that the same applies to other nonlinear viscoelastic models.

It is often more convenient to work with the dimensionless form of Eq. 27. Introducing the normalizations $\bar{y}=y/H$ and $\bar{\kappa}=\kappa H$, we can write the dimensionless velocity profile as

$$\begin{aligned}
\frac{u}{u_{\mathrm{sh}}} &= \overline{\dot{\gamma}}_1(\overline{y}+1)\left(1+2\overline{\dot{\gamma}}_1^{-2}\frac{\varepsilon\mathrm{De}_\kappa^2}{\overline{\kappa}^2}\right)-\left(1+6\overline{\dot{\gamma}}_1^{-2}\frac{\varepsilon\mathrm{De}_\kappa^2}{\overline{\kappa}^2}\right)\overline{\Omega}^-_{1,1}(\overline{y})\\
&\quad+2\overline{\dot{\gamma}}_1\frac{\varepsilon\mathrm{De}_\kappa^2}{\overline{\kappa}}\left(6\Psi_1\Psi_2\overline{\kappa}(\overline{y}+1)+\frac{3}{2}\overline{\Omega}^-_{2,1}(\overline{y})\right)-2\varepsilon\mathrm{De}_\kappa^2\left(\frac{1}{3}\overline{\Omega}^-_{3,1}(\overline{y})+3\Psi_1\Psi_2\overline{\Omega}^-_{1,1}(\overline{y})\right)\\
&\quad+\frac{1}{2}\Gamma\left(\overline{y}^2-1\right)\left(1+6\overline{\dot{\gamma}}_1^{-2}\frac{\varepsilon\mathrm{De}_\kappa^2}{\overline{\kappa}^2}+\frac{\varepsilon\mathrm{De}_\kappa^2}{\overline{\kappa}^2}\Gamma^2\left(\overline{y}^2+1\right)\right)+2\overline{\dot{\gamma}}_1\frac{\varepsilon\mathrm{De}_\kappa^2}{\overline{\kappa}^2}\Gamma^2\left(\overline{y}^3+1\right)\\
&\quad-12\overline{\dot{\gamma}}_1\frac{\varepsilon\mathrm{De}_\kappa^2}{\overline{\kappa}^3}\Gamma\left(\overline{\Omega}^-_{1,2}(\overline{y})-\overline{\Omega}^+_{1,1}(\overline{y})\right)+6\frac{\varepsilon\mathrm{De}_\kappa^2}{\overline{\kappa}^2}\Gamma\left(\Psi_1\Psi_2\overline{\kappa}^2\left(\overline{y}^2-1\right)+\frac{1}{2}\overline{\Omega}^-_{2,2}(\overline{y})-\frac{1}{4}\overline{\Omega}^+_{2,1}(\overline{y})\right)\\
&\quad-6\frac{\varepsilon\mathrm{De}_\kappa^2}{\overline{\kappa}^4}\Gamma^2\left(\overline{\Omega}^-_{1,3}(\overline{y})+2\overline{\Omega}^-_{1,1}(\overline{y})-2\overline{\Omega}^+_{1,2}(\overline{y})\right),
\end{aligned} \tag{32}$$

where $\overline{\Omega}^{\pm}_{p,q}(y)$ is the normalized version of the operator introduced by (28), defined as

$$\overline{\Omega}^{\pm}_{p,q}(\overline{y})=(\overline{\kappa}\,\overline{y})^{(q-1)}\,\overline{\Omega}^{\pm}_{p}(\overline{y})-(-1)^{(q+1)}\overline{\kappa}^{(q-1)}\overline{\Omega}^{\pm}_{p}(-1), \tag{33}$$

with $\overline{\Omega}^{\pm}_{p}(\overline{y})=\Psi_1^p\left(\mathrm{e}^{\overline{\kappa}\,\overline{y}}\right)^p\pm\Psi_2^p\left(\mathrm{e}^{-\overline{\kappa}\,\overline{y}}\right)^p$.

The dimensionless shear-rate asymmetry coefficient can be calculated from

$$\overline{\dot{\gamma}}_1^3 + \overline{a}_1\overline{\dot{\gamma}}_1^2 + \overline{a}_2\overline{\dot{\gamma}}_1 + \overline{a}_3 = 0, \tag{34}$$

with coefficients

$$\begin{aligned}
\overline{a}_1 &= -\frac{3}{2}\overline{\Omega}_{1,1}^-(1),\\
\overline{a}_2 &= \frac{\overline{\kappa}^2}{2\varepsilon \mathrm{De}_\kappa^2} + \Gamma^2 + 6\overline{\kappa}^2\Psi_1\Psi_2 + \frac{3}{4}\overline{\kappa}\overline{\Omega}_{2,1}^-(1) - 3\frac{\Gamma}{\overline{\kappa}}\left(\overline{\Omega}_{1,2}^-(1) - \overline{\Omega}_{1,1}^+(1)\right),\\
\overline{a}_3 &= -\frac{1}{4}\frac{\overline{\kappa}^2\overline{\Omega}_{1,1}^-(1)}{\varepsilon \mathrm{De}_\kappa^2} - \frac{1}{2}\overline{\kappa}^2\left(\frac{1}{3}\overline{\Omega}_{3,1}^-(1) + 3\Psi_1\Psi_2\overline{\Omega}_{1,1}^-(1)\right) + \frac{3}{2}\Gamma\left(\frac{1}{2}\overline{\Omega}_{2,2}^-(1) - \frac{1}{4}\overline{\Omega}_{2,1}^+(1)\right)\\
&\quad -\frac{3}{2}\frac{\Gamma^2}{\overline{\kappa}^2}\left(\overline{\Omega}_{1,3}^-(1) + 2\overline{\Omega}_{1,1}^-(1) - 2\overline{\Omega}_{1,2}^+(1)\right),
\end{aligned} \tag{35}$$

where $\overline{\dot{\gamma}}_1 = \frac{\dot{\gamma}_1 H}{u_{\mathrm{sh}}}$ and $\mathrm{De}_\kappa = \frac{\lambda u_{\mathrm{sh}}}{\xi} = \lambda\kappa u_{\mathrm{sh}}$ is the Deborah number based on the EDL thickness and on the Helmholtz–Smoluchowski electro-osmotic velocity, defined as $u_{\mathrm{sh}} = -\frac{\epsilon\zeta_1 E_x}{\eta}$ [11]. In Poiseuille flows a different Deborah number is usually defined [15] based on the cross-sectional average velocity for the Newtonian flow under the sole influence of pressure gradient and the channel half-height, $\mathrm{De}_N = \frac{\lambda U_N}{H}$ with $U_N = -\frac{H^2 p_{,x}}{3\eta}$. A third alternative Deborah number for electro-osmotic flow is based again on u_{sh}, but considers the channel half-height, $\mathrm{De}_{\mathrm{sh}} = \frac{\lambda u_{\mathrm{sh}}}{H}$. These three Deborah numbers are related by $\mathrm{De}_\kappa = \bar{\kappa}\mathrm{De}_{\mathrm{sh}} = -\frac{3}{\Gamma}\bar{\kappa}\mathrm{De}_N$, where parameter $\Gamma = -\frac{H^2}{\epsilon\zeta_1}\frac{p_{,x}}{E_x}$ represents the ratio of pressure to electro-osmotic driving forces. Note that for simplicity the above terms were based on the zeta potential at the bottom wall, ($\psi_{\|y=-H} = \zeta_1$), but can be related with the upper-wall zeta potential using the ratio of zeta potentials: $u_{\mathrm{sh}} = u_{\mathrm{sh}2}/R_\zeta$, $\Gamma = R_\zeta\Gamma_2$ and $\mathrm{De}_\kappa = \mathrm{De}_{\kappa 2}/R_\zeta$. The solution of Eq. 34 is similar to Eq. 30. The flow rate per unit length can be determined from integration of the velocity profile (27). Here, this integration was carried out using the normalized velocity profile, Eq. 32, leading to the following expression

$$\begin{aligned}
\overline{Q} = \frac{Q}{2Hu_{\mathrm{sh}}} = \frac{\overline{u}}{u_{\mathrm{sh}}} &= \frac{1}{2}\int_{-1}^{1}\frac{u}{u_{\mathrm{sh}}}\mathrm{d}\bar{y} = \overline{\dot{\gamma}}_1\left(1 + 2\frac{\varepsilon\mathrm{De}_\kappa^2}{\overline{\kappa}^2}\overline{\dot{\gamma}}_1^2\right) - \frac{1}{2}\Gamma\left(\frac{4}{5}\frac{\varepsilon\mathrm{De}_\kappa^2}{\overline{\kappa}^2}\Gamma^2 + \frac{2}{3}\left(1 + 6\overline{\dot{\gamma}}_1^2\frac{\varepsilon\mathrm{De}_\kappa^2}{\overline{\kappa}^2}\right)\right)\\
&\quad + 2\overline{\dot{\gamma}}_1\frac{\varepsilon\mathrm{De}_\kappa^2}{\overline{\kappa}^2}\Gamma^2 - \frac{1}{2}\left(1 + 6\frac{\varepsilon\mathrm{De}_\kappa^2}{\overline{\kappa}^2}\overline{\dot{\gamma}}_1^2\right)\left(\frac{\overline{\Omega}_{1,1}^+(1)}{\overline{\kappa}} - 2\overline{\Omega}_1^-(-1)\right)\\
&\quad + \frac{\varepsilon\mathrm{De}_\kappa^2}{\overline{\kappa}}\overline{\dot{\gamma}}_1\left(12\Psi_1\Psi_2\overline{\kappa} + \frac{3}{2}\left(\frac{\overline{\Omega}_{2,1}^+(1)}{2\overline{\kappa}} - 2\overline{\Omega}_2^-(-1)\right)\right)\\
&\quad - \varepsilon\mathrm{De}_\kappa^2\left(\frac{\overline{\Omega}_{3,1}^+(1)}{9\overline{\kappa}} - \frac{2}{3}\overline{\Omega}_3^-(-1) + 3\Psi_1\Psi_2\left(\frac{\overline{\Omega}_{1,1}^+(1)}{\overline{\kappa}} - 2\overline{\Omega}_1^-(-1)\right)\right)\\
&\quad - 6\overline{\dot{\gamma}}_1\frac{\varepsilon\mathrm{De}_\kappa^2}{\overline{\kappa}^4}\Gamma\left[\overline{\Omega}_{1,2}^+(1) - 2\overline{\Omega}_{1,1}^-(1) + 2\overline{\kappa}\left(\overline{\kappa}\overline{\Omega}_1^-(-1) + \overline{\Omega}_1^+(-1)\right)\right]\\
&\quad + 3\frac{\varepsilon\mathrm{De}_\kappa^2}{\overline{\kappa}^2}\Gamma\left(\frac{1}{4\overline{\kappa}}\left(\overline{\Omega}_{2,2}^+(1) - \overline{\Omega}_{2,1}^-(1)\right) - \frac{4}{3}\Psi_1\Psi_2\overline{\kappa}^2 + \overline{\kappa}\overline{\Omega}_2^-(-1) + \frac{1}{2}\overline{\Omega}_2^+(-1)\right)\\
&\quad - 3\frac{\varepsilon\mathrm{De}_\kappa^2}{\overline{\kappa}^5}\Gamma^2\left(\overline{\Omega}_{1,3}^+(1) - 4\overline{\Omega}_{1,2}^-(1) + 6\overline{\Omega}_{1,1}^+(1)\right)\\
&\quad + 6\frac{\varepsilon\mathrm{De}_\kappa^2}{\overline{\kappa}^4}\Gamma^2\left(\left(\overline{\kappa}^2 + 2\right)\overline{\Omega}_1^-(-1) + 2\overline{\kappa}\overline{\Omega}_1^+(-1)\right).
\end{aligned} \tag{36}$$

The decoupling of this total flow rate into its three fundamental contributions (pure electro-osmosis, pure Poiseuille flow and the nonlinear combined forcing contribution) is not attempted here since it leads to extremely complex

relations, if at all possible. In fact, the dependence on the *shear-rate asymmetry coefficient*, $\overline{\dot{\gamma}}_1$, complicates this task, because $\overline{\dot{\gamma}}_1$ is the solution given by (30) of the cubic equation (29), and each of its various component coefficients ($\overline{a}_1$, $\overline{a}_2$ and $\overline{a}_3$) also contain the same fundamental contributions. However, it is possible to gain insight into this issue by looking at the simpler symmetric case for which Afonso et al. [6] quantified the relative flow-rate contributions (cf. their Fig. 10). For instance, for large viscoelasticity ($\sqrt{\varepsilon}\mathrm{De}_\kappa \geq 5$), the ratio of flow rates asymptotes and becomes inversely proportional to $\overline{\kappa}$. If the double layer is thick, say $\overline{\kappa} = 20$, and for a favourable pressure gradient, $\overline{Q}_{EP}/\overline{Q}_T$ can be of the order of 19%, decreasing to 4% for a thin EDL. This nonlinear contribution becomes stronger than the pure Poiseuille contribution at high values of $\sqrt{\varepsilon}\mathrm{De}_\kappa$, even if the pressure gradient is adverse.

The explicit expressions for the dimensionless shear and normal-stress components are obtained from normalization of (24) and (25):

$$\frac{\tau_{xy}}{3\eta u_{\mathrm{sh}}\kappa} = \frac{1}{3}\left[\Gamma\frac{\overline{y}}{\overline{\kappa}} + \frac{\overline{\dot{\gamma}}_1}{\overline{\kappa}} - \overline{\Omega}_1^+(\overline{y})\right], \tag{37}$$

$$\frac{\tau_{xx}}{3\eta u_{\mathrm{sh}}\kappa} = \frac{2}{3}\mathrm{De}_\kappa\left[\Gamma\frac{\overline{y}}{\overline{\kappa}} + \frac{\overline{\dot{\gamma}}_1}{\overline{\kappa}} - \overline{\Omega}_1^+(\overline{y})\right]^2. \tag{38}$$

The normalized shear rate is

$$\frac{\dot{\gamma}}{u_{\mathrm{sh}}\kappa} = \left[1 + 2\varepsilon\mathrm{De}_\kappa^2\left(\Gamma\frac{\overline{y}}{\overline{\kappa}} + \frac{\overline{\dot{\gamma}}_1}{\overline{\kappa}} - \overline{\Omega}_1^+(\overline{y})\right)^2\right]\left(\Gamma\frac{\overline{y}}{\overline{\kappa}} + \frac{\overline{\dot{\gamma}}_1}{\overline{\kappa}} - \overline{\Omega}_1^+(\overline{y})\right) \tag{39}$$

and the viscosity profile can be obtained from

$$\mu(\dot{\gamma}) \equiv \frac{\tau_{xy}}{\dot{\gamma}} \Rightarrow \frac{\mu(\dot{\gamma})}{\eta} = \left[1 + 2\varepsilon\mathrm{De}_\kappa^2\left(\Gamma\frac{\overline{y}}{\overline{\kappa}} + \frac{\overline{\dot{\gamma}}_1}{\overline{\kappa}} - \overline{\Omega}_1^+(\overline{y})\right)^2\right]^{-1}. \tag{40}$$

3.4 Analytical solution for the FENE-P model

As pointed out at the end of Sect. 3.2, for fully developed channel flow, there is similarity between the solutions for the sPTT and the FENE-P models [16]. By comparing (16) and (17) for the sPTT model with (19) and (20) for the FENE-P model, and since the momentum equation (23) is independent of the constitutive equation, an exact equivalence in the sense of a parameter-to-parameter match is obtained, as explained in detail in [17]. Hence, the solution of Sect. 3.3 and Appendix A also applies to the flow of FENE-P fluids, provided the following substitutions are made:

$$\begin{aligned} f(\tau_{xx}) &\rightarrow \left(\frac{b+2}{b+5}\right) Z(\tau_{xx}),\\ \lambda &\rightarrow \lambda\left(\frac{b+2}{b+5}\right),\\ \varepsilon &\rightarrow \frac{1}{b+5},\\ \eta &\rightarrow \eta. \end{aligned} \tag{41}$$

4 Discussion of results

In Sect. 3 the solution was obtained for fully developed flow of viscoelastic fluids (sPTT and FENE-P fluids) under the mixed influence of pressure gradient and electro-osmosis induced by asymmetric zeta potentials at the channel

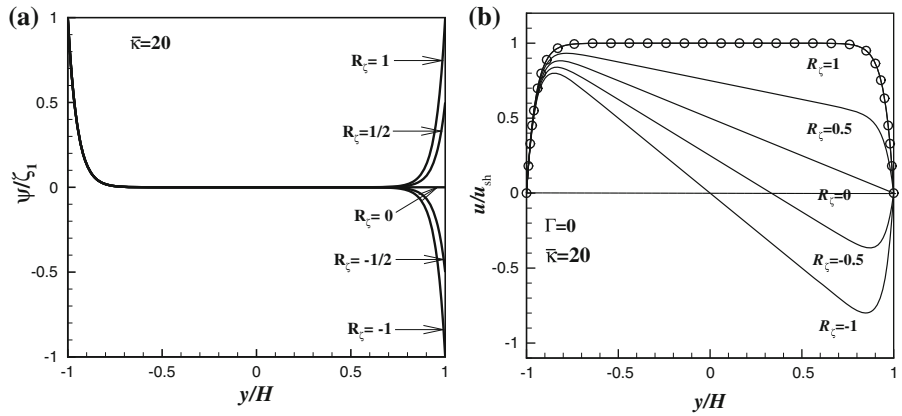

Fig. 2 Effect of zeta-potential ratio on Newtonian flow under pure electro-osmosis ($\Gamma = 0$) and $\bar{\kappa} = 20$: **a** Dimensionless potential and **b** velocity profiles. *Symbols* in (**b**) represent the data from Burgreen and Nakache [20]

walls. The different influences of the driving forces, fluid rheology and zeta-potential ratio on the velocity profiles have been identified in (27); in this section we discuss in detail some of the various limiting cases in order to better understand the fluid dynamics. The limit cases contained in the general solution are: (a) Newtonian fluid with mixed electro-osmotic/pressure driving forces and asymmetric wall zeta potentials; (b) Pure electro-osmotic flows of viscoelastic fluids with asymmetric wall zeta potentials; (c) Poiseuille flow of a viscoelastic fluid and (d) Viscoelastic fluid with mixed electro-osmotic/pressure driving forces and asymmetric wall zeta potentials. Case (c) was studied in detail elsewhere [15–18], and so was case (a) in [1], but this latter situation is revisited here as a starting point.

4.1 Newtonian fluid with mixed driving forces and asymmetric zeta potentials

For a Newtonian fluid the relaxation time is zero, so the Deborah number vanishes ($\mathrm{De}_\kappa = 0$), and Eq. 32 becomes

$$\frac{u}{u_{\mathrm{sh}}} = \overline{\dot{\gamma}}_1 \left(\overline{y} + 1\right) - \overline{\Omega}^{-}_{1,1}(\overline{y}) + \tfrac{1}{2}\Gamma\left(\overline{y}^2 - 1\right), \tag{42}$$

under the mixed influence of electro-osmotic and pressure driving forces, as was also shown by Soong and Wang [1]. As explained in Sect. 3.3, the asymmetric boundary-conditions for the zeta potential at the channel walls introduces a new constant in the velocity profile, $\overline{\dot{\gamma}}_1$, that depends on the ratio of zeta potentials, R_ζ, on the relative microchannel ratio, $\bar{\kappa}$, on the ratio of pressure gradient to electro-osmotic driving forces, Γ, and on the fluid rheology. For a Newtonian fluid the dimensionless *shear-rate asymmetry coefficient* is a linear function of R_ζ, as expressed by $\overline{\dot{\gamma}}_1 = \frac{1}{2}\overline{\Omega}^{-}_{1,1}(1) = \frac{1}{2}\left(R_\zeta - 1\right)$. For symmetric boundary conditions ($R_\zeta = 1$), $\overline{\dot{\gamma}}_1 = 0$, and the velocity profile is simplified to that of Dutta and Beskok [19]. For $\Gamma \to \infty$, pressure forces dominate the momentum transport for any value of $\bar{\kappa}$, and the classical laminar parabolic velocity profile is recovered. Note that this corresponds to $E_x \to 0$ and $u_{\mathrm{sh}} \to 0$, since $u_{\mathrm{sh}} \propto E_x$ and $\Gamma \propto E_x^{-1}$. For $\Gamma \to 0$, the last term on the right-hand side of (42) vanishes, the flow becomes governed exclusively by electro-osmosis and the velocity profile is a function of the wall distance, the relative microchannel ratio, $\bar{\kappa}$, and the ratio of zeta potentials, R_ζ, as shown by Soong and Wang [1]. So, for symmetric boundary conditions ($R_\zeta = 1$), the velocity profile is only a function of the wall distance and the relative microchannel ratio, $\bar{\kappa}$, as shown earlier by Burgreen and Nakache [20]. Note that for large $\bar{\kappa}$ ($\bar{\kappa} \to \infty$) the size of the EDL, or region of excess charge, is relatively small, and (42) reduces to the classical Helmoltz–Smoluchowski equation, $u/u_{\mathrm{sh}} = 1$ [11], if simultaneously $\Gamma = 0$.

Figure 2a shows the effect of the ratio of zeta potentials, R_ζ, on the variation of the dimensionless potential for pure electro-osmotic flow ($\Gamma = 0$) and relative microchannel ratio of $\bar{\kappa} = 20$. When the ratio of zeta potentials

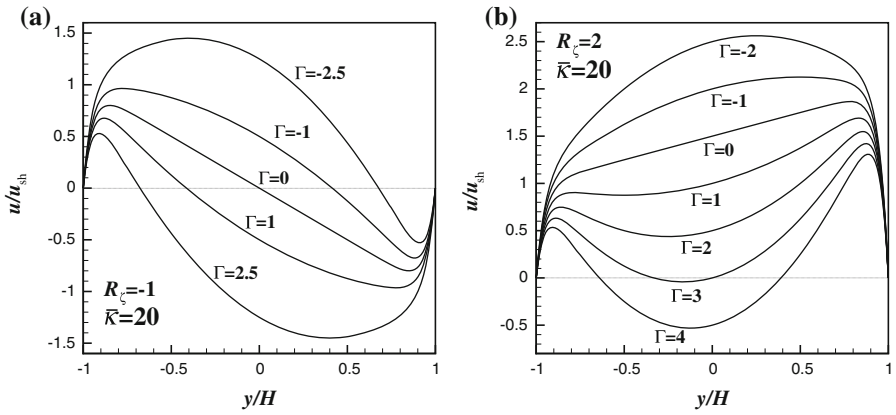

Fig. 3 Velocity profiles for Newtonian fluids for $\bar{\kappa} = 20$ and different ratios of pressure to electro-osmotic driving forces, Γ, and zeta potential ratios: **a** $R_\zeta = -1$ and **b** $R_\zeta = 2$

decreases from symmetric ($R_\zeta = 1$) to anti-symmetric ($R_\zeta = -1$) the corresponding dimensionless potential profiles vary from fully symmetric to fully anti-symmetric, respectively. This is also observed in the velocity profiles presented in Fig. 2b: for symmetric boundary conditions ($R_\zeta = 1$) the velocity profile corresponds to a *pluglike flow*, as shown earlier by Burgreen and Nakache [20]. When $R_\zeta = -1$ the velocity profiles are fully anti-symmetric.

Figure 3 shows Newtonian velocity profiles for various ratios of pressure gradient to electro-osmotic driving forces at $\bar{\kappa} = 20$ and for different values of R_ζ. When $\Gamma = 0$ and $R_\zeta = -1$ the velocity profiles are anti-symmetric, as seen in Fig. 2b. When $\Gamma \neq 0$, corresponding to mixed Poiseuille electro-osmotic flows, the pressure-gradient effect can be observed in the favorable ($\Gamma < 0$) or adverse ($\Gamma > 0$) contributions for the velocity profiles. The velocity profiles shown in Fig. 3b for $\bar{\kappa} = 20$ and $R_\zeta = 2$, show a *skewed pluglike* profile, due to a higher zeta potential at $\overline{y} = 1$. Equation 42 predicts negative velocities at $\bar{y} = 0$ when $\Gamma > 2\overline{\dot{\gamma}}_1 - \left[\frac{R_\zeta + 1 - 2\cosh(\bar{\kappa})}{\cosh(\bar{\kappa})}\right]$ for all values of $\bar{\kappa}$ and R_ζ. For symmetric boundary conditions, negative velocities at $\bar{y} = 0$ are predicted for $\Gamma > 2$ and small but finite Debye lengths, $\bar{\kappa} \gtrsim 10$, as observed by Afonso et al. [6].

4.2 Viscoelastic fluid with pure electro-osmosis and asymmetric zeta potential

For the sPTT fluid under pure electro-osmosis driving force, the solution is derived by setting $\Gamma = 0$, for which Eq. 32 reduces to

$$\frac{u}{u_{\text{sh}}} = \overline{\dot{\gamma}}_1 (\overline{y} + 1)\left(1 + 2\overline{\dot{\gamma}}_1^2 \frac{\varepsilon \text{De}_\kappa^2}{\overline{\kappa}^2}\right) - \left(1 + 6\overline{\dot{\gamma}}_1^2 \frac{\varepsilon \text{De}_\kappa^2}{\overline{\kappa}^2}\right)\overline{\Omega}_{1,1}^-(\overline{y}) + 2\overline{\dot{\gamma}}_1 \frac{\varepsilon \text{De}_\kappa^2}{\overline{\kappa}}\left(6\Psi_1\Psi_2\overline{\kappa}(\overline{y} + 1) + \frac{3}{2}\overline{\Omega}_{2,1}^-(\overline{y})\right) - 2\varepsilon \text{De}_\kappa^2\left(\frac{1}{3}\overline{\Omega}_{3,1}^-(\overline{y}) + 3\Psi_1\Psi_2\overline{\Omega}_{1,1}^-(\overline{y})\right). \quad (43)$$

For symmetric boundary conditions ($R_\zeta = 1$ and $\overline{\dot{\gamma}}_1 = 0$) the above equation reduces to that presented by Afonso et al. [6], but for $R_\zeta \neq 1$ the dimensionless *shear-rate asymmetry coefficient*, $\overline{\dot{\gamma}}_1$, depends on the fluid rheological properties, as shown in Fig. 4a. For $R_\zeta < 1$, $\overline{\dot{\gamma}}_1$ is always negative, decreasing with the increase of $\sqrt{\varepsilon}\text{De}_\kappa$, an indication that the shear stress is also decreasing as $\sqrt{\varepsilon}\text{De}_\kappa$ increases. For $R_\zeta > 1$, $\overline{\dot{\gamma}}_1$ is always positive and increases with $\sqrt{\varepsilon}\text{De}_\kappa$, since increasing the shear-thinning behaviour of the fluid, leads to higher shear stresses. All curves asymptote to the same limiting curve when $\sqrt{\varepsilon}\text{De}_\kappa \to \infty$, with the absolute value of $\overline{\dot{\gamma}}_1$ increasing when $\bar{\kappa}$ increases ($\bar{\kappa} = 20$, 100, 150 and 200), as observed in Fig. 4b. The increase of $\overline{\dot{\gamma}}_1$ with $\bar{\kappa}$ is related with the reduction

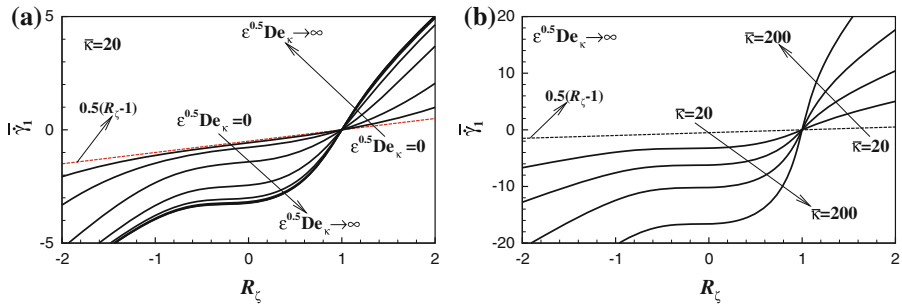

Fig. 4 Variation of the dimensionless *shear-rate asymmetry coefficient*, $\bar{\dot{\gamma}}_1$, for purely electro-osmotic viscoelastic flow ($\Gamma = 0$) as a function of the ratio of zeta potentials, R_ζ. **a** Increasing $\sqrt{\varepsilon}\mathrm{De}_\kappa$ for $\bar{\kappa} = 20$ and **b** asymptotic limit for $\sqrt{\varepsilon}\mathrm{De}_\kappa \to \infty$ at several $\bar{\kappa}$

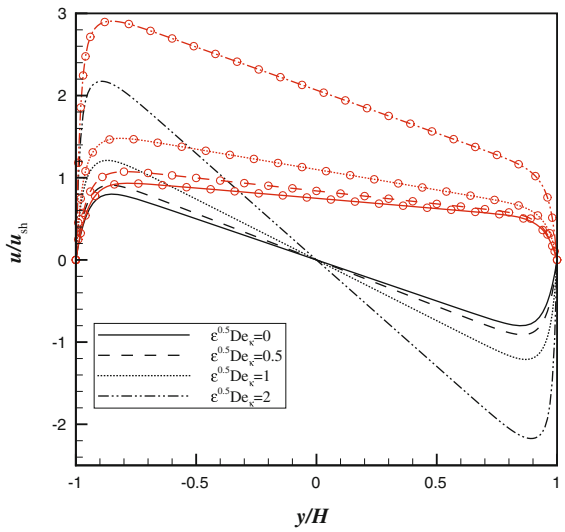

Fig. 5 Dimensionless velocity profiles as a function of $\sqrt{\varepsilon}\mathrm{De}_\kappa$ for electro-osmotic flow ($\Gamma = 0$) of a PTT fluid for $R_\zeta = -1$ (*lines*) and $R_\zeta = 0.5$ (*lines with symbols*) at relative microchannel ratios of $\bar{\kappa} = 20$

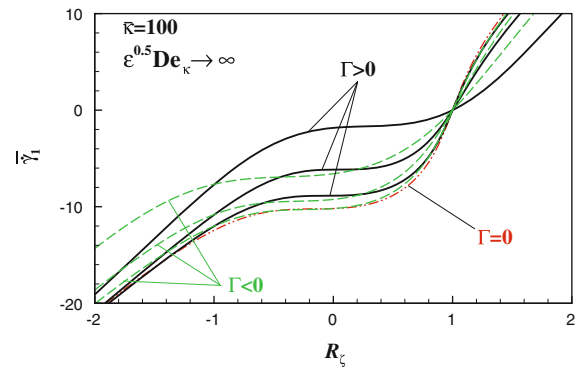

Fig. 6 Variation of the dimensionless *shear-rate asymmetry coefficient*, $\bar{\dot{\gamma}}_1$, with R_ζ as a function of Γ (electro-osmotic/pressure-driven flow) for the asymptotic limit of $\sqrt{\varepsilon}\mathrm{De}_\kappa \to \infty$ and $\bar{\kappa} = 100$

of the shear layer thicknesses, leading to high shear stresses near the wall, i.e., higher values of $\bar{\dot{\gamma}}_1$ are needed to balance the velocity profile.

Figure 5 shows the corresponding dimensionless velocity profiles as a function of the parameter $\sqrt{\varepsilon}\mathrm{De}_\kappa$ for two ratios of zeta potentials, $R_\zeta = -1$ and $R_\zeta = 0.5$, and a relative microchannel ratio of $\bar{\kappa} = 20$. These profiles should be compared with those in Fig. 2b pertaining to Newtonian fluids. As for Newtonian fluids, the velocity profiles for $R_\zeta = -1$ exhibit an *anti-symmetric pluglike* shape (full lines in Fig. 5), with the absolute velocities increasing with $\sqrt{\varepsilon}\mathrm{De}_\kappa$. For $R_\zeta = 0.5$, increasing $\sqrt{\varepsilon}\mathrm{De}_\kappa$ also leads to an increase in the *skewed pluglike* profile, as observed in Fig. 5. This flow enhancement by increasing $\sqrt{\varepsilon}\mathrm{De}_\kappa$ is typical of sPTT fluids and is associated with the increased shear-thinning behaviour of the fluid.

4.3 Viscoelastic fluid with mixed driving forces and asymmetric zeta potentials

The viscoelastic flow characteristics under the combined action of electro-osmosis and a pressure gradient are discussed in this section following (32).

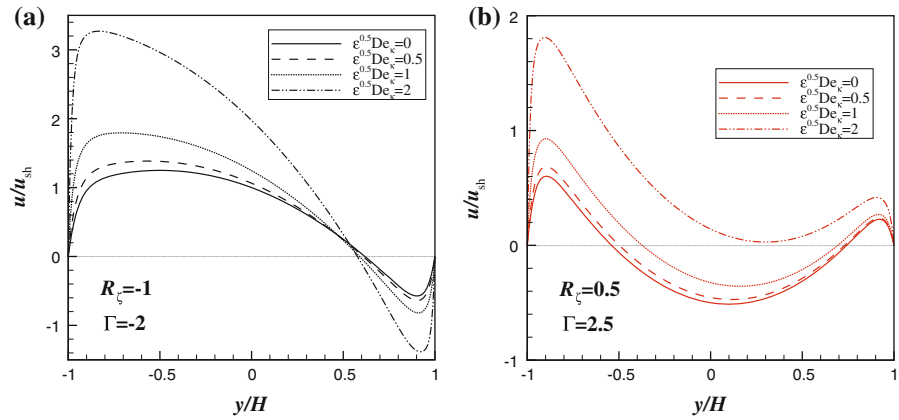

Fig. 7 Dimensionless velocity profiles for a PTT fluid under the mixed influence of electro-osmotic/pressure driving force as function of $\sqrt{\varepsilon}\mathrm{De}_\kappa$ for relative microchannel ratio of $\bar{\kappa} = 20$: **a** $\Gamma = -2$ and $R_\zeta = -1$ and **b** $\Gamma = 2.5$ and $R_\zeta = 0.5$

The Poiseuille effect on the dimensionless *shear-rate asymmetry coefficient*, $\overline{\dot{\gamma}}_1$, is presented in Fig. 6, here for the asymptotic limit of $\sqrt{\varepsilon}\mathrm{De}_\kappa \to \infty$. By increasing the favorable pressure gradient (decreasing Γ), $\overline{\dot{\gamma}}_1$ increases, especially for $R_\zeta < 1$. By increasing Γ for adverse pressure gradient conditions, $\overline{\dot{\gamma}}_1$ also increases, especially for $-1 < R_\zeta < 1$, i.e., $\overline{\dot{\gamma}}_1$ behaves monotonically but nonlinearly with R_ζ showing the minimum value for $R_\zeta < 1$ and the maximum for $R_\zeta > 1$. Figure 7 (a) and (b) present the dimensionless velocity profiles for the flows with favorable and adverse pressure gradients, respectively. For $\Gamma < 0$ with anti-symmetric zeta potentials ($R_\zeta = -1$), the velocity profiles increase with $\sqrt{\varepsilon}\mathrm{De}_\kappa$, due to shear-thinning effects, leading to correspondingly higher shear rates near the walls. For $\Gamma > 0$ with $R_\zeta = 0.5$, the velocity profiles show the same double peak seen for Newtonian flows (cf. Fig. 3a), due to the retarding action of the pressure gradient. The velocity profiles also increase with $\sqrt{\varepsilon}\mathrm{De}_\kappa$, again due to shear-thinning effects, both within the EDL layer and in the bulk zone.

In Appendix A the streaming-potential solution induced by Poiseuille flow is presented and discussed.

5 Conclusions

Analytical solutions for channel flow of symmetric z–z electrolyte viscoelastic fluids under the mixed influence of electro-osmosis and pressure gradient forcings were obtained for the case of asymmetric wall zeta potentials. This analysis is restricted to cases with small electric double-layers, where the wall-to-wall distance is at least one order of magnitude larger than the thickness of each EDL. The viscoelastic fluids analysed are described by the sPTT model with linear kernel for the stress-coefficient function and zero second normal-stress difference [7], and the FENE-P model [9]. In addition, we have also presented the solution for the streaming potential. The solution remains valid for the particular combination of forcings known as the streaming potential and the flow characteristics are determined by the same equations provided $E_x = E_{x,\mathrm{sp}}$ and $\Gamma = \Gamma_{\mathrm{sp}}$, where Γ_{sp} and $E_{x,\mathrm{sp}}$ are given in Appendix A.

Acknowledgements The authors acknowledge funding from FEDER and Fundação para a Ciência e a Tecnologia (FCT), Portugal, through projects PTDC/EQU-FTT/70727/2006 and PTDC/EQU-FTT/71800/2006. A.M. Afonso would also like to thank FCT for financial support through scholarship SFRH/BD/28828/2006.

Appendix A: Streaming-potential solution

In the solution presented in Sect. 3, the electrical field E_x can be applied externally or be a consequence of electric potentials created by the flow. In the absence of an externally applied electrical field, the applied pressure difference

induces a flow carrying ions that generate an electrical current, called the streaming current, I_s'. The streaming current accumulates counterions at the end of the channel therefore setting up an electric field, $E_{x,\mathrm{sp}}$ which is associated with the so-called streaming potential, ϕ_{sp} via $E_{x,\mathrm{sp}} = -\Delta\phi_{\mathrm{sp}}/l$. This induced electric field creates an opposite current, I_c', called conduction current which induces a flow contrary to the pressure-induced flow. This is established in such way that under steady state conditions the net electrical current, I', vanishes. The net electric current is the sum of the streaming currents and the electrical conduction current:

$$I' = I_s' + I_c' \equiv 0. \tag{A.1}$$

The electrical streaming current (per unit of width) is of the form:

$$I_s' = \int_{-H}^{H} u(y)\rho_e(y)\mathrm{d}y = \int_{-H}^{H} -u(y)\epsilon\kappa^2\zeta_1\Omega_1^-(y)\mathrm{d}y, \tag{A.2}$$

which for the sPTT fluid leads to

$$\begin{aligned}
\frac{I_s'}{\epsilon\zeta_1} = {} & -\dot{\gamma}_1\left(1+2\varepsilon\lambda^2\dot{\gamma}_1^2\right)\left(2\overline{\kappa}\Omega_1^+(H)-\Omega_{1,1}^-(H)\right)+6\varepsilon\lambda^2\left[\frac{\epsilon E_{x,\mathrm{sp}}\zeta_1}{\eta}\right]^2\kappa^2\dot{\gamma}_1\Psi_1\Psi_2\left(2\Omega_{1,1}^-(H)-4\overline{\kappa}\Omega_1^+(H)\right)\\
& -\frac{1}{2}\left[\frac{\epsilon E_{x,\mathrm{sp}}\zeta_1}{\eta}\right]\left(1+6\dot{\gamma}_1^2\varepsilon\lambda^2\right)\kappa\left(\Omega_2^-(H)+\Omega_2^-(-H)-2\Psi_1\Psi_2\left(4\overline{\kappa}+\mathrm{e}^{-2\overline{\kappa}}-\mathrm{e}^{2\overline{\kappa}}\right)-2\Psi_1^2+2\Psi_2^2\right)\\
& +\varepsilon\lambda^2\left[\frac{\epsilon E_{x,\mathrm{sp}}\zeta_1}{\eta}\right]^2\kappa^2\dot{\gamma}_1\left[-\Omega_3^-(H)-2\Omega_3^-(-H)+3\Psi_1\Psi_2\left(\Omega_1^-(H)-2\Omega_1^-(-H)\right)\right.\\
& \left.+3\left(\Psi_1^3\mathrm{e}^{-\overline{\kappa}}-\Psi_2^3\mathrm{e}^{\overline{\kappa}}+\Psi_1^2\Psi_2\mathrm{e}^{-3\overline{\kappa}}-\Psi_1\Psi_2^2\mathrm{e}^{3\overline{\kappa}}\right)\right]\\
& +\frac{1}{6}\varepsilon\lambda^2\left[\frac{\epsilon E_{x,\mathrm{sp}}\zeta_1}{\eta}\right]^3\kappa^3\left[-\Omega_4^-(H)-3\Omega_4^-(-H)+2\Psi_1\Psi_2\left(\Omega_2^-(H)-3\Omega_2^-(-H)\right)\right.\\
& \left.+4\left(\Psi_1^4\mathrm{e}^{-2\overline{\kappa}}-\Psi_2^4\mathrm{e}^{2\overline{\kappa}}+\Psi_1^3\Psi_2\mathrm{e}^{-4\overline{\kappa}}-\Psi_1\Psi_2^3\mathrm{e}^{4\overline{\kappa}}\right)\right]\\
& +6\varepsilon\lambda^2\left[\frac{\epsilon E_{x,\mathrm{sp}}\zeta_1}{\eta}\right]^3\kappa^3\Psi_1\Psi_2\left(\Psi_1^2-\Psi_2^2-\frac{1}{2}\left(\Omega_2^-(H)+\Omega_2^-(-H)\right)+\Psi_1\Psi_2\left(4\overline{\kappa}+\mathrm{e}^{-2\overline{\kappa}}-\mathrm{e}^{2\overline{\kappa}}\right)\right)\\
& +\left[\frac{p_{,x}}{\eta}\right]\frac{1}{\kappa}\left(1+6\varepsilon\lambda^2\dot{\gamma}_1^2\right)\left(\Omega_{1,2}^-(H)-\Omega_{1,1}^+(H)\right)\\
& +2\frac{\varepsilon\lambda^2}{\kappa^3}\left[\frac{p_{,x}}{\eta}\right]^3\left[\Omega_{1,4}^-(H)-3\Omega_{1,3}^+(H)+6\Omega_{1,2}^-(H)-6\Omega_{1,1}^+(H)\right]-2\frac{\dot{\gamma}_1\varepsilon\lambda^2}{\kappa^2}\left[\frac{p_{,x}}{\eta}\right]^2\left[2\overline{\kappa}^3\Omega_1^+(H)\right.\\
& \left.-3\Omega_{1,3}^-(H)+6\Omega_{1,2}^+(H)-6\Omega_{1,1}^-(H)\right]-3\varepsilon\lambda^2\left[\frac{\epsilon E_{x,\mathrm{sp}}\zeta_1}{\eta}\right]\left[\frac{p_{,x}}{\eta}\right]\dot{\gamma}_1\left[2\overline{\kappa}\Omega_{2,1}^-(H)-3\Omega_2^+(H)-\Omega_2^+(-H)\right]\\
& -12\varepsilon\lambda^2\left[\frac{\epsilon E_{x,\mathrm{sp}}\zeta_1}{\eta}\right]\left[\frac{p_{,x}}{\eta}\right]\dot{\gamma}_1\left[\Psi_1\Psi_2\left(-2+\mathrm{e}^{-2\overline{\kappa}}\left(1+\overline{\kappa}\right)+\mathrm{e}^{2\overline{\kappa}}\left(1-\overline{\kappa}\right)\right)+\Psi_1^2\left(1+\overline{\kappa}\right)+\Psi_2^2\left(1-\overline{\kappa}\right)\right]\\
& -\frac{1}{2}\frac{\varepsilon\lambda^2\left[\frac{\epsilon E_{x,\mathrm{sp}}\zeta_1}{\eta}\right]\left[\frac{p_{,x}}{\eta}\right]^2}{\kappa}\left[6\overline{\kappa}\Omega_{2,2}^-(H)-6\Omega_{2,2}^+(H)+3\Omega_{2,1}^-(H)\right.\\
& \left.+12\left(\Psi_1\Psi_2\left(-\frac{4}{3}\overline{\kappa}^3-\overline{\kappa}^2\mathrm{e}^{-2\overline{\kappa}}+\overline{\kappa}^2\mathrm{e}^{2\overline{\kappa}}\right)+\overline{\kappa}^2\Psi_2^2-\overline{\kappa}^2\Psi_1^2\right)\right]\\
& -6\frac{\varepsilon\lambda^2\left[\frac{\epsilon E_{x,\mathrm{sp}}\zeta_1}{\eta}\right]\left[\frac{p_{,x}}{\eta}\right]^2}{\kappa}\left[\Omega_2^-(H)+\Omega_2^-(-H)+\Psi_1\Psi_2\left(-8\overline{\kappa}-2\mathrm{e}^{-2\overline{\kappa}}+2\mathrm{e}^{2\overline{\kappa}}\right)\right.\\
& \left.+2\Psi_2^2-2\Psi_1^2-\frac{1}{2}\left(2\overline{\kappa}\Omega_{2,1}^+(H)-\Omega_{2,1}^-(H)\right)\right]
\end{aligned}$$

$$+12\frac{\varepsilon\lambda^2\left[\frac{\epsilon E_{x,\mathrm{sp}}\zeta_1}{\eta}\right]\left[\frac{p_{,x}}{\eta}\right]^2}{\kappa}\left[\overline{\kappa}\Psi_1\Psi_2\left(-2+\mathrm{e}^{-2\overline{\kappa}}+\mathrm{e}^{2\overline{\kappa}}\right)+\overline{\kappa}\Psi_2^2+\overline{\kappa}\Psi_1^2\right]$$
$$-12\frac{\varepsilon\lambda^2}{\kappa}\left[\frac{\epsilon E_{x,\mathrm{sp}}\zeta_1}{\eta}\right]^2\left[\frac{p_{,x}}{\eta}\right]\Psi_1\Psi_2\kappa^2\left(-\Omega_{1,2}^-(H)+\Omega_{1,1}^+(H)\right)$$
$$-\frac{1}{6}\varepsilon\lambda^2\kappa\left[\frac{\epsilon E_{x,\mathrm{sp}}\zeta_1}{\eta}\right]^2\left[\frac{p_{,x}}{\eta}\right]\left[-5\Omega_3^+(H)-4\Omega_3^+(-H)+6\overline{\kappa}\Omega_3^-(H)\right.$$
$$\left.-12\overline{\kappa}\Omega_3^-(-H)+\Psi_1\Psi_2\left(27\Omega_1^+(H)-36\Omega_1^+(-H)-18\overline{\kappa}\Omega_1^-(H)-36\overline{\kappa}\Omega_1^-(-H)\right)\right]$$
$$-\frac{3}{2}\varepsilon\lambda^2\kappa\left[\frac{\epsilon E_{x,\mathrm{sp}}\zeta_1}{\eta}\right]^2\left[\frac{p_{,x}}{\eta}\right]\left[(2\overline{\kappa}+1)\left(\Psi_1^2\Psi_2\mathrm{e}^{-3\overline{\kappa}}+\Psi_1^3\mathrm{e}^{-\overline{\kappa}}\right)+(1-2\overline{\kappa})\left(\Psi_1\Psi_2^2\mathrm{e}^{3\overline{\kappa}}+\Psi_2^3\mathrm{e}^{\overline{\kappa}}\right)\right]. \quad \text{(A.3)}$$

In Eq. A.3 the electric potential E_x has already been substituted by the corresponding streaming potential, $E_{x,\mathrm{sp}}$. The electrical conduction current in the channel is defined as:

$$I_c' = 2H\sigma_t E_{x,\mathrm{sp}}, \quad \text{(A.4)}$$

where σ_t is the total electric conductivity. Note that the conduction current can now flow back through both the fluid as well as the channel walls, depending on the corresponding electrical conductivities. The total electrical conductivity can be calculated as $\sigma_t = \sigma_{\mathrm{fluid}} + \sigma_{\mathrm{sur}} P_{\mathrm{sur}}/A_{\mathrm{chan}}$, where P_{sur} and A_{chan} are the wetting perimeter and cross-section area of the channel, respectively and σ_{fluid} and σ_{sur} are the fluid bulk and wall surface conductivities, respectively. Upon substitution of Eqs. A.3 and A.4 we arrive at an algebraic cubic equation in the streaming potential field as function of the imposed pressure gradient. This cubic equation has a real solution given in Eq. 30 as well as in classical books; cf [21, pp. 178–180]. This cubic equation in $E_{x,\mathrm{sp}}$ can alternatively be written in non-dimensional form to give Γ_{sp}, where $\Gamma_{\mathrm{sp}} = -\frac{H^2}{\epsilon\zeta_1}\frac{p_{,x}}{E_{x,\mathrm{sp}}}$. In this case, it is customary [6,12] to normalize the electric conductivity σ_t as Υ_1, defined as $\Upsilon_1 = \frac{H^2\eta\sigma_t}{\epsilon^2\zeta_1^2}$.

References

1. Soong CY, Wang SH (2003) Theoretical analysis of electrokinetic flow and heat transfer in a microchannel under asymmetric boundary conditions. J Colloid Interface Sci 265:202–213
2. Nguyen N-T, Wereley ST (2006) Fundamentals and applications of microfluidics, chap 3: fabrication techniques in microfluidics, 2nd edn. Artech House, Boston, USA
3. Kuo A-T, Chang C-H, Wei H-H (2008) Transient currents in electrolyte displacement by asymmetric electro-osmosis and determination of surface zeta potentials of composite microchannels. Appl Phys Lett 92:244102
4. Islam N, Wu J (2006) Microfluidic transport by AC electroosmosis. J Phys Conf Ser 34:356–361
5. Mansuripur TS, Pascall AJ, Squires TM (2009) Asymmetric flows over symmetric surfaces: capacitive coupling in induced-charge electro-osmosis. New J Phys 11:075030
6. Afonso AM, Alves MA, Pinho FT (2009) Analytical solution of mixed electro-osmotic/pressure driven flows of viscoelastic fluids in microchannels. J Non-Newtonian Fluid Mech 159:50–63
7. Phan-Thien N, Tanner RI (1977) New constitutive equation derived from network theory. J Non-Newtonian Fluid Mech 2:353–365
8. Phan-Thien N (1978) A non-linear network viscoelastic model. J Rheol 22:259–283
9. Bird RB, Dotson PJ, Johnson NL (1980) Polymer solution rheology based on a finitely extensible bead-spring chain model. J Non-Newtonian Fluid Mech 7:213–235
10. Dhinakaran S, Afonso AM, Alves MA, Pinho FT (2010) Steady viscoelastic fluid flow between parallel plates under electro-osmotic forces: Phan-Thien Tanner model. J Colloid Interface Sci 344:513–520
11. Park HM, Lee WM (2008) Helmholtz–Smoluchowski velocity for viscoelastic electroosmotic flows. J Colloid Interface Sci 317:631–636
12. Sousa JJ, Afonso AM, Pinho FT, Alves MA (2010) Effect of the skimming-layer on electro-osmotic—Poiseuille flows of viscoelastic fluids. Microfluid Nanofluid. doi:10.1007/s10404-010-0651-y
13. Sousa PC, Pinho FT, Oliveira MSN, Alves MA (2010) Efficient microfluidic rectifiers for viscoelastic fluid flow. J Non-Newtonian Fluid Mech 165:652–671
14. Bruus H (2008) Theoretical microfluidics, Oxford master series in Condensed matter physics. Oxford University Press, Oxford, UK

15. Oliveira PJ, Pinho FT (1999) Analytical solution for fully developed channel and pipe flow of Phan-Thien–Tanner fluids. J Non-Newtonian Fluid Mech 387:271–280
16. Oliveira PJ (2002) An exact solution for tube and slit flow of a FENE-P fluid. Acta Mech 158:157–167
17. Cruz DOA, Pinho FT, Oliveira PJ (2005) Analytical solutions for fully developed laminar flow of some viscoelastic liquids with a Newtonian solvent contribution. J Non-Newtonian Fluid Mech 132:28–35
18. Alves MA, Pinho FT, Oliveira PJ (2001) Study of steady pipe and channel flows of a single-mode Phan Thien–Tanner fluid. J Non-Newtonian Fluid Mech 101:55–76
19. Dutta P, A Beskok (2001) Analytical solution of combined electroosmotic /pressure driven flows in two-dimensional straight channels: finite debye layer effects. Anal Chem 73:1979–1986
20. Burgreen D, Nakache FR (1964) Electrokinetic flow in ultrafine capillary slits. J Phys Chem 68:1084–1091
21. Press WH, Flannery PP, Teukolsky SA, Vetterling WT (1992) Numerical recipes in Fortran: the art of scientific computing. 2nd Edn, Cambridge University Press